Diversity-Oriented Stapling Yields Intrinsically Cell-Penetrant Inducers of Autophagy

Leila Peraro,[†] Zhongju Zou,[‡,§] Kamlesh M. Makwana,[†] Ashleigh E. Cummings,[†] Haydn L. Ball,[‡] Hongtao Yu,[†] Yu-Shan Lin,[†] Beth Levine,[*,‡,§,‖] and Joshua A. Kritzer[*,†]

[†]Department of Chemistry, Tufts University, Medford, Massachusetts 02155, United States,

[‡]Center for Autophagy Research, Department of Internal Medicine, [§]Howard Hughes Medical Institute, and [‖]Department of Microbiology, University of Texas Southwestern Medical Center, Dallas, Texas 75390, United States

S *Supporting Information*

ABSTRACT: Autophagy is an essential pathway by which cellular and foreign material are degraded and recycled in eukaryotic cells. Induction of autophagy is a promising approach for treating diverse human diseases, including neurodegenerative disorders and infectious diseases. Here, we report the use of a diversity-oriented stapling approach to produce autophagy-inducing peptides that are intrinsically cell-penetrant. These peptides induce autophagy at micromolar concentrations in vitro, have aggregate-clearing activity in a cellular model of Huntington's disease, and induce autophagy in vivo. Unexpectedly, the solution structure of the most potent stapled peptide, DD5-o, revealed an α-helical conformation in methanol, stabilized by an unusual ($i,i+3$) staple which cross-links two D-amino acids. We also developed a novel assay for cell penetration that reports exclusively on cytosolic access and used it to quantitatively compare the cell penetration of DD5-o and other autophagy-inducing peptides. These new, cell-penetrant autophagy inducers and their molecular details are critical advances in the effort to understand and control autophagy. More broadly, diversity-oriented stapling may provide a promising alternative to polycationic sequences as a means for rendering peptides more cell-penetrant.
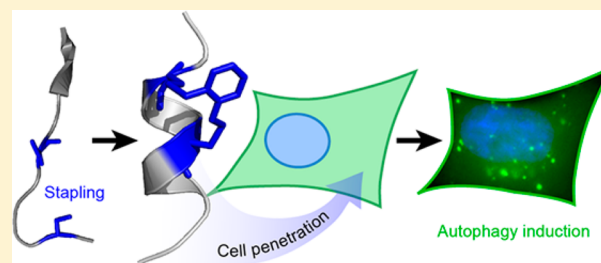
INTRODUCTION

Macroautophagy (hereafter referred to as autophagy) is a coordinated process by which eukaryotic cells recycle material, including bulk cytosol, damaged organelles, protein aggregates, and invading organisms.[1,2] It is an evolutionarily conserved pathway in all eukaryotes and is fundamental for cellular survival and development.[3] Autophagy is initiated in the cytosol, where cellular or foreign material becomes engulfed by a double-membrane vesicle called the autophagosome (Figure 1a). Autophagosomes are then trafficked to the lysosome, where they fuse with the lysosomal membrane and release their contents for enzymatic breakdown.[4]

Impaired autophagy is a hallmark of many human diseases. Protein aggregation, a common feature of many neurodegenerative disorders including Alzheimer's, Parkinson's, and Huntington's, has been linked to reduced initiation of autophagy and impaired fusion of autophagosomes to lysosomes.[5] Down-regulation of autophagy has also been implicated in tumorigenesis.[6–9] Loss-of-function studies in mice and other model organisms demonstrate a crucial role for autophagy in protein and organelle quality control,[10] metabolism,[11] innate and adaptive immunity,[12] protection against aging,[13] and a wide range of diseases.[14–16] Because impaired autophagy is prominent in the pathogenesis and pathology of so many conditions, pharmacological activation of autophagy has been proposed as a promising avenue for new

treatments.[17–20] While some existing drugs enhance autophagy,[15] they have pleiotropic effects, and it is not known whether their clinical benefits are mediated by autophagy. Thus, more selective molecules are highly sought after to test autophagy activation as a therapeutic mode for many different conditions.

The molecular pathways that control autophagy are an intense area of current study, and the protein complexes and mechanisms involved have yet to be fully elucidated. However, it is known that the protein Beclin 1 is a master regulator of autophagy (Figure 1a).[6,16] When autophagy is triggered, Beclin 1 forms a large multiprotein complex with a class III phosphatidylinositol 3-kinase, and this complex nucleates autophagosome formation.[16,21] Beclin 1 interacts with several known positive and negative regulators of autophagy, including Bcl-2/Bcl-x$_L$, AMBRA1, rubicon, DAPK, AKT, EGFR, MAPAPK2/3, UVRAG, golgi-associated plant pathogenesis-related protein 1 (GAPR-1), and HIV-Nef, highlighting its critical role in the control of autophagy.[16,22–24]

To date, one of the most potent, selective inducers of autophagy is the peptide Tat-Beclin 1, which was derived from the sequence of Beclin 1 (Figure 1b,c). While its molecular target is unknown, Tat-Beclin 1 activates Beclin 1 and the core autophagy initiation complex, in a manner that antagonizes the
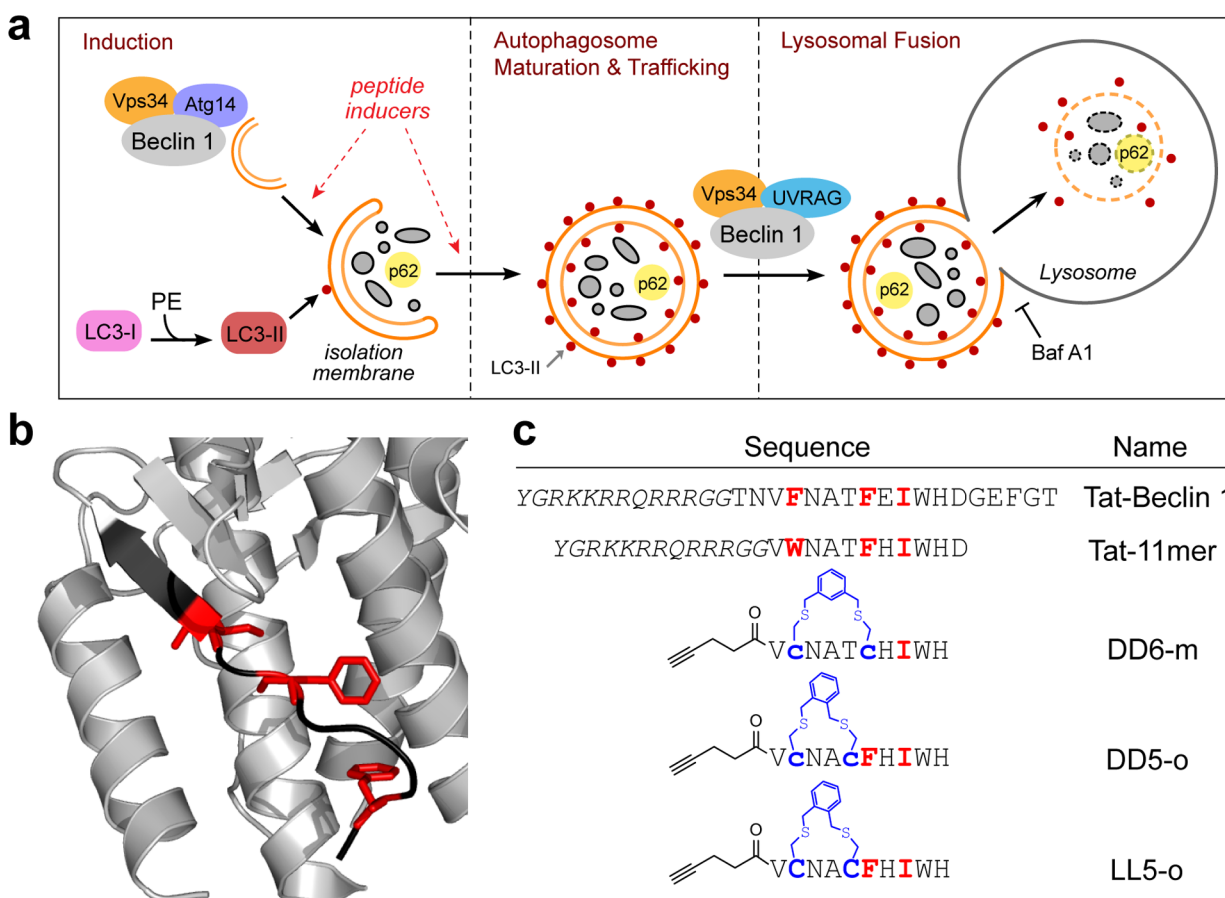
Figure 1. The autophagic pathway and peptide inducers of autophagy. (a) Overall schematic of the process of autophagy. In response to upstream signaling, Beclin 1 and its PI3K complex (which includes lipid kinase subunit Vps34 and regulatory subunit Atg14) nucleate membrane formation. The microtubule-associated protein light chain I (LC3-I) becomes lipidated with phosphatidylethanolamine (PE). The lipidated form, LC3-II, is then incorporated in autophagosome membranes. The autophagosome matures, fully engulfs the cargo, and is trafficked to the lysosome where it fuses with the lysosomal membrane. This maturation process is controlled by a different Beclin 1 complex, involving the regulator UVRAG. Following lysosomal fusion, autophagosomes and their contents, including the autophagy adaptor protein p62, are broken down and recycled. Peptide inducers appear to act during the induction phase (red dashed arrows). Bafilomycin A1 (Baf A1) is a known inhibitor of the lysosomal fusion step. (b) Crystal structure of the ECD of human Beclin 1.[44] The segment shown in black corresponds to the sequence of the Beclin 1-derived portion of Tat-11mer, and the red residues correspond to the required hot spots for Tat-11mer activity. (c) Sequences of autophagy-inducing peptides, with conserved hot spot residues highlighted in red. The cysteine residues and linkers are highlighted in blue, and lowercase c denotes D-cysteine.

effects of the negative regulator GAPR-1.[23] It has also been shown to be effective in numerous in vitro and in vivo models of human disease.[25−34] Thus, Tat-Beclin 1 has become a powerful tool to explore the mechanism of autophagy initiation and the effect of autophagy on disease. However, it has inherent liabilities for drug development, including its large size, its composition as a peptide with all natural amino acids, and its inability to enter cells without the polycationic Tat sequence. While Tat-linked peptides have been explored as potential therapeutics, there remain concerns with their overall distribution properties, efficacy, and toxicity.[35] Thus, despite the broad adoption of Tat-Beclin 1 as a tool compound, the development of Tat-independent autophagy inducers represents an important milestone for translation into human therapeutics.

There are no direct strategies for removing a polycationic transducing sequence from a bioactive peptide while retaining cell penetration and activity. Our laboratory and others have shown that, in specific cases, conformational constraints can increase the potency, metabolic stability, and cell penetration of bioactive peptides.[36−39] Many successful strategies have employed side-chain-to-side-chain covalent cross-linking, or "stapling". Current stapling chemistries include ring-closing olefin metathesis, lactam formation, oxime linkages, and azide−alkyne cycloaddition,[40] but the low-yielding nature of many macrocyclization reactions can limit the throughput and conformational diversity available.[41]

Here we used thiol bis-alkylation to produce stapled versions of the Beclin 1 peptide that retain bioactivity without the Tat sequence. Because the structure of the bioactive peptide was unknown, we used a diversity-oriented stapling strategy (Figure 2a).[42,43] Also, we devised a novel cell penetration assay to quantitatively measure cytosolic delivery. This assay demonstrated the intrinsically cell-penetrant nature of the new stapled peptides.

■ RESULTS

Design and Synthesis of Improved Tat-Linked Peptides. The autophagy-inducing peptide Tat-Beclin 1 (Figure 1c) was derived from the sequence of the evolutionarily conserved domain (ECD) of Beclin 1 (Figure 1b).[23,44] First, we
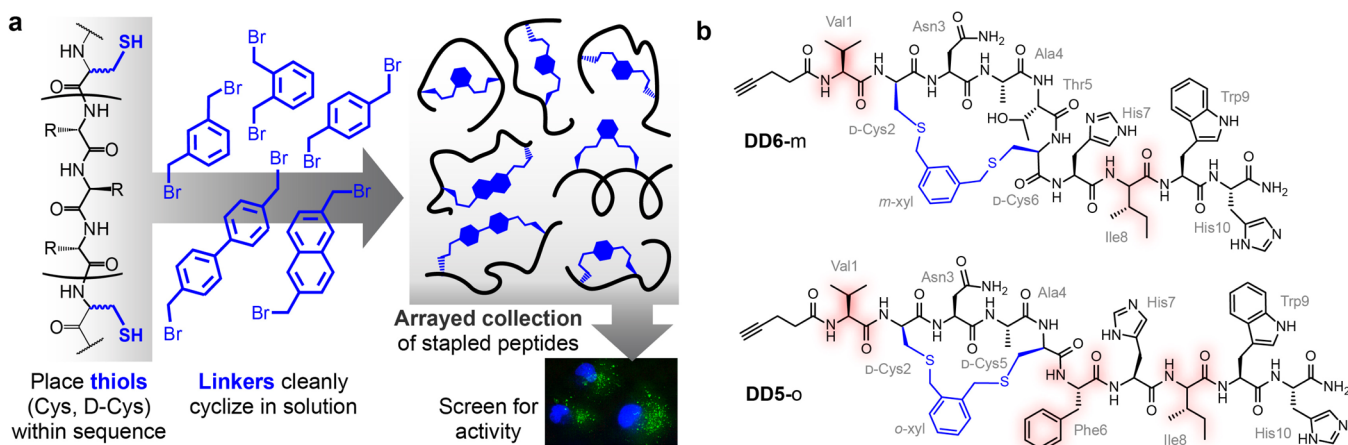
Figure 2. Diversity-oriented stapling approach. (a) General strategy for diversity-oriented stapling, here applied to produce stapled analogues of Beclin 1-derived sequences for testing in cell-based autophagy assays. Pairs of thiol-containing amino acids were introduced at various positions within the sequence and reacted with a variety of dibromide linkers to yield an array of conformationally diverse stapled peptides, which were then screened for activity. (b) Chemical structures of peptides DD6-m and DD5-o. Residues are numbered and labeled in gray, linkers are denoted in blue, and the conserved hot spot residues are highlighted in red.

defined the minimal active portion of Tat-Beclin 1 by testing analogues in autophagy assays in HeLa cells. Observing dose-dependent degradation of p62 with a corresponding increase in LC3-I conversion to LC3-II, both measured by Western blot, is a rigorous standard for concluding that autophagy is being induced.[45,46] When autophagic flux is especially strong, LC3-II is degraded more rapidly than it is produced, leading to lower overall levels of LC3-I and LC3-II; we would expect to see this result for more potent autophagy inducers at higher concentrations.[45,46] Truncations of two residues from the N-terminus of the Beclin-derived sequence and five residues from the C-terminus yielded a Tat-linked peptide with improved activity (SI Figure 2). Further substitutions of Glu7 to His (reverting this position to the wild-type residue) and Phe2 to Trp (a conservative substitution) led to an optimized peptide called Tat-11mer (Figure 1c, SI Figure 2). Tat11-mer consisted of 11 residues derived from Beclin 1, with a Gly-Gly linker and Tat sequence on the N-terminus. Further truncation of Tat-11mer's Beclin-derived sequence by one residue on either terminus produced peptides with similar activity (SI Figure 2). An alanine scan of Tat-11mer revealed that Trp2, Phe6, and Ile8 in the Beclin 1-derived region were necessary for activity (SI Figure 3). This correlates with previous data for full-length Tat-Beclin 1, where altering the residues that correspond to Trp2 and Phe6 completely abolished activity.[23] Tat-11mer is approximately 2-fold more potent than the previously reported Tat-Beclin 1, with a robust increase in autophagy observed in cell culture at 5 μM.

The peptide pa-11mer, which lacks Tat and has an N-terminus capped with pentynoic acid (SI Table 1), did not induce autophagy (Figure 3a). Because truncation of the C-terminal aspartate did not affect the activity of Tat-11mer (SI Figure 2), we removed it from pa-11mer to produce pa-10mer. This peptide had inconclusive results in immunoblot assays (some p62 degradation but little LC3 conversion was observed, Figure 3a), but results from an orthogonal autophagic flux assay more conclusively showed pa10-mer has a very mild effect on autophagy (SI Figure 4).
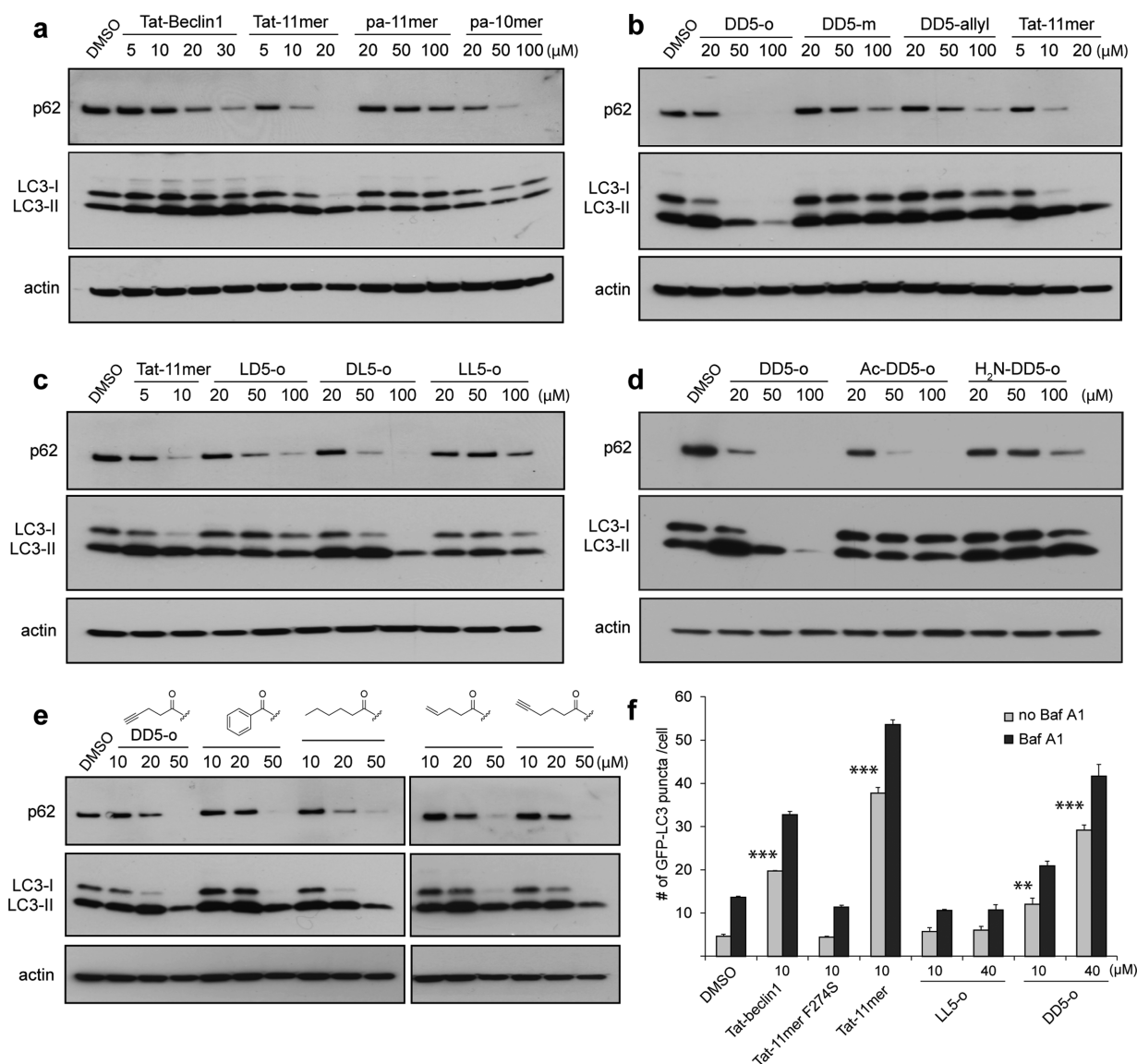
Stapled Peptides Induce Autophagic Flux in Vitro. The 10-mer sequence has no negative charges and induces autophagy when linked to Tat, so it was a suitable starting point

for peptide stapling. Tat-Beclin 1 did not have canonical helical, sheet, or turn structure based on structural or modeling data,[23] so it was not possible to predict which stapled conformations would yield peptides that retained activity. We therefore employed a diversity-oriented stapling strategy (Figure 2a). In this approach, we introduced two thiol-containing amino acids within the sequence and used thiol bis-alkylation to cross-link them.[47] This cross-linking reaction can be performed in solution under mild aqueous conditions and has proven to be very robust and relatively insensitive to macrocycle conformation.[48−52] For all the stapled peptides described herein, we observed nearly quantitative yields and little formation of dimer or other side products.[52] The location of the staple was varied and included locations that are proximal to each other in the crystal structure of the ECD of Beclin 1 (Figure 1b). For each staple position, all permutations of L- and D-cysteines were tested, along with a variety of different linkers. In this manner, a synthetic panel of peptides with varied conformational constraints was produced for testing in cell-based autophagy assays. A unique aspect of this strategy is that it does not presume a specific target structure, which allowed us to search broadly for a stapled conformation that promotes cell penetration and autophagy-inducing activity.

While many stapled analogues of pa-10mer were inactive (SI Figure 5), substituting Trp2 and Phe6 with D-cysteines and cross-linking with m-xylene yielded a peptide with improved activity (peptide DD6-m, shown in Figure 2b, which showed strong autophagy induction at 100 μM; see SI Figure 6). A significant improvement in activity was observed when the staple was altered from an (i,i+4) spacing to an (i,i+3) spacing by substituting Trp2 and Thr5 with D-cysteines, and cross-linking with o-xylene. This peptide, DD5-o, has potent in vitro activity at 20 μM (Figure 3b).

The diversity-oriented stapling strategy provided ample evidence that the activity of the stapled peptides was dependent on conformation. For instance, the o-xylene cross-linked DD5-o induced autophagy, whereas isomers of DD5-o that were cross-linked with m- and p-xylene (DD5-m and DD5-p) did not. This suggested that activity required not just macrocyclization but the specific shape conferred by the o-xylene linker. Similarly, the m-xylene cross-linked DD6-m was capable of inducing

Figure 3. Peptides induce autophagy in HeLa cells and increase autophagic flux. Autophagy induction in HeLa cells was measured by treating cells with the indicated concentration of each peptide for 2 h, and then analyzing p62 degradation and LC3 lipidation (conversion of LC3-I to lipidated LC3-II) by immunoblot. Actin is shown as a loading control (a−e). (a) At 5 μM, Tat-11mer induced autophagy to a similar extent as Tat-beclin 1 at 10 μM. Removing Tat and capping the N-terminus (pa-11mer; sequence in SI Table 1) led to loss of activity. Further truncation of the C-terminal Asp (pa-10mer) led to minimal activity at 100 μM. (b) Autophagy induction is dependent on linker conformation. DD5-o induced autophagy at 20 μM, while DD5-m, which has a *m*-xylene instead of *o*-xylene, and DD5-allyl, which is not stapled and instead has an allyl group on each D-cysteine, did not induce autophagy. (c) Autophagy induction depends on the stereochemistry of the linker cysteines. DD5-o was the most active stereoisomer, while the stereoisomer with two L-cysteines, LL5-o, had minimal autophagy-inducing activity. (d) The N-terminal cap affects activity. DD5-o has a 4-pentynyl cap. When this cap is changed to an acetyl cap or a free amine, almost no autophagy-inducing activity is observed. (e) Many variants of DD5-o, with a variety of N-terminal caps, were evaluated (see SI Figure 7 for additional cap variants). (f) The GFP-LC3 puncta assay in HeLa cells provides an independent measure of autophagic flux. GFP-LC3 HeLa cells were treated with and without bafilomycin A1 (Baf A1), which leads to accumulation of autophagosomes. For a−f, similar results were obtained in at least three independent experiments. Bars represent mean ± SEM for triplicate samples (at least 100 cells analyzed per sample). ** denotes $P < 0.01$ and *** denotes $P < 0.001$ by t test for indicated group vs DMSO control.

autophagy, while *o*- and *p*-xylene variants were not (SI Figure 6). Activity was also dependent on the stereochemistry of the linker cysteines. Among stereoisomers of DD5-o, only the variant with two D-cysteines robustly increased autophagy. The L/D and D/L stereoisomers mildly increased autophagy, and almost no increase was observed for the stereoisomer with two L-cysteines (Figure 3c; very mild activity was observed at 100 μM). The L/L stereoisomer (LL5-o) was thus used as a negative control in subsequent experiments. All together, these data

showed that the activity of DD5-o depends on conformation, which in turn demonstrates the value of a diversity-oriented approach to peptide stapling.

The activity of DD5-o was also dependent on the N-terminal cap. DD5-o was capped with 4-pentynoic acid, but when analogues with free or acetylated N-termini were tested, we observed little to no activity (some p62 degradation but little LC3 conversion is observed for these peptides; Figure 3d). This led us to test a panel of alkyl and aryl N-terminal caps (Figure
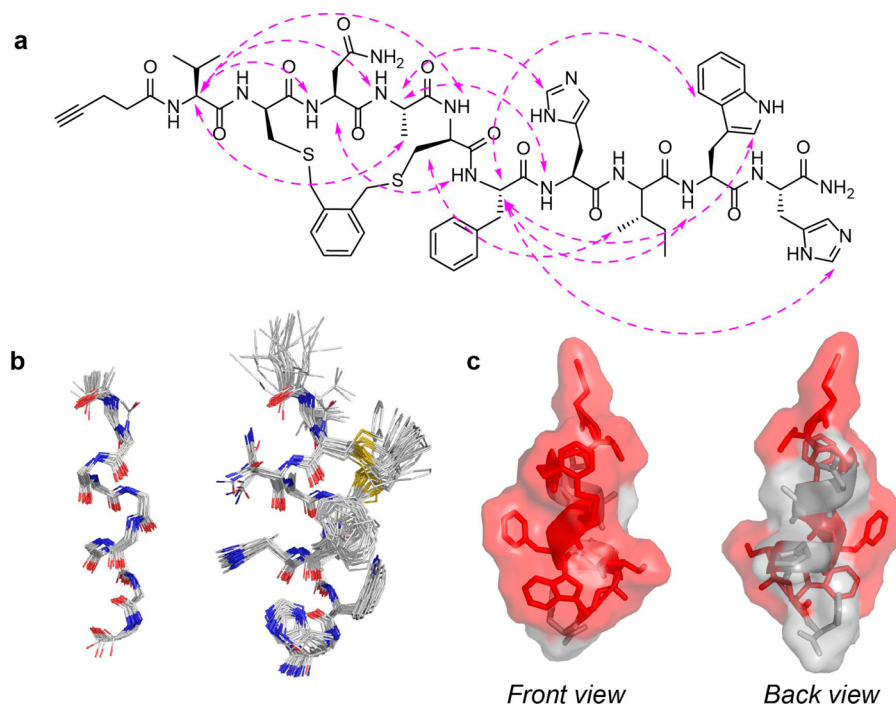
Figure 4. Solution structure of DD5-o. (a) Diagram showing medium-range and long-range NOEs used for structure determination of DD5-o. Complete assignments, NOEs and simulation details are provided in Supporting Information. (b) Ensemble of 25 lowest-energy solution structures showing the overlay of the backbone only (left) and backbone with side chains (right). Backbone RMSD for this overlay was 0.44 Å, and all-heavy-atom RMSD was 1.1 Å. (c) Surface representation of DD5-o. Hot spot residues, linker and cap are highlighted in red. Front view (left) shows the extended hydrophobic surface on one face of the peptide, which includes the hot spot residues. Rear view (right) shows residues found to be nonessential for activity (gray).

3e and SI Figure 7). Analogues with pentenyl, hexanyl, 3-cyanopropanyl, and hexynyl caps induced autophagy but to a somewhat lesser extent than DD5-o (SI Figure 7). Among peptides capped with aryl groups, an analogue with a benzoic acid cap induced autophagy to a slightly lesser extent than DD5-o, but highly similar peptides with phenylacetic acid and nicotinic acid caps showed no activity.

An alanine scan was also performed on DD5-o to determine which residues are important for autophagy-inducing activity. Substituting Val1, Phe6, or Ile8 with Ala led to complete loss of activity (SI Figure 8). Substituting Trp9 or His10 with Ala led to significantly decreased activity, while substituting Asn3 or His7 led to milder effects on activity. These data largely matched the alanine-scan data for Tat-11mer, demonstrating conservation of the hot spot residues and suggesting that they share a common mechanism of action. The requirement for Val1, however, is unique to DD5-o. This suggests that Val1, and perhaps the N-terminal cap, may have direct effects on cell penetration.

Autophagy was measured in an additional in vitro assay to confirm that Tat-11mer and DD5-o truly induced autophagic flux, rather than blocking autophagosome maturation or lysosomal function. HeLa cells stably expressing GFP-LC3 were treated with peptide for 2 h in serum-free media, and the number of GFP-LC3 puncta per cell were counted using fluorescence microscopy.[23] These experiments were also performed in the presence of bafilomycin A1 (Baf A1), which prevents the fusion of autophagosomes with lysosomes by inhibiting vacuolar H⁺ ATPase (Figure 1a).[53] Autophagy induction causes an increase in numbers of autophagosomes per cell (quantifiable as GFP-LC3 puncta), which further increase when Baf A1 blocks lysosomal fusion.[54] In this assay,

we observed autophagy induction for both Tat-11mer and DD5-o at 10 μM. Comparing extent of autophagy induction at 10 μM, DD5-o had slightly less activity than Tat-Beclin 1, and Tat-11mer had nearly twice the activity of Tat-Beclin 1 (Figure 3f). All three peptides produced a further increase in GFP-LC3 puncta upon cotreatment with Baf A1, confirming true increases in autophagic flux. These results match the p62 and LC3 immunoblot data and are consistent with the model that Beclin 1-derived peptides activate autophagy at the level of enhanced autophagosome formation and/or maturation.[23]

Solution Structure of DD5-o in Methanol. The in vitro data suggested that the stapled peptides required a specific 3D conformation. However, it was unclear what this conformation might be. The crystal structure of the ECD of Beclin 1 is composed of three consecutive β-sheet-α-helix autophagy-specific (BARA) motifs.[44] Published data have highlighted the importance of the ECD in the architecture of the autophagy initiation complex, though its role is not fully understood.[55,56] The sequence of the ECD corresponding to the autophagy-inducing peptides is at the edge of the region that was crystallized and shows no regular secondary structure (Figure 1b).[44] The amino acid composition and the relative positioning of hot spot residues were also not suggestive of a specific preferred secondary structure. Thus, it was unclear what structure this segment assumes in any relevant biological context.

While DD5-o was not soluble enough in water for 2D-NMR experiments, we were able to use 2D-NMR spectroscopy to determine the structure of DD5-o in methanol (Figure 4). The 1D proton spectrum was well-resolved with excellent dispersion among the amide protons (SI Figure 9). Two-dimensional COSY, TOCSY, and ROESY were recorded (SI Figures 10–
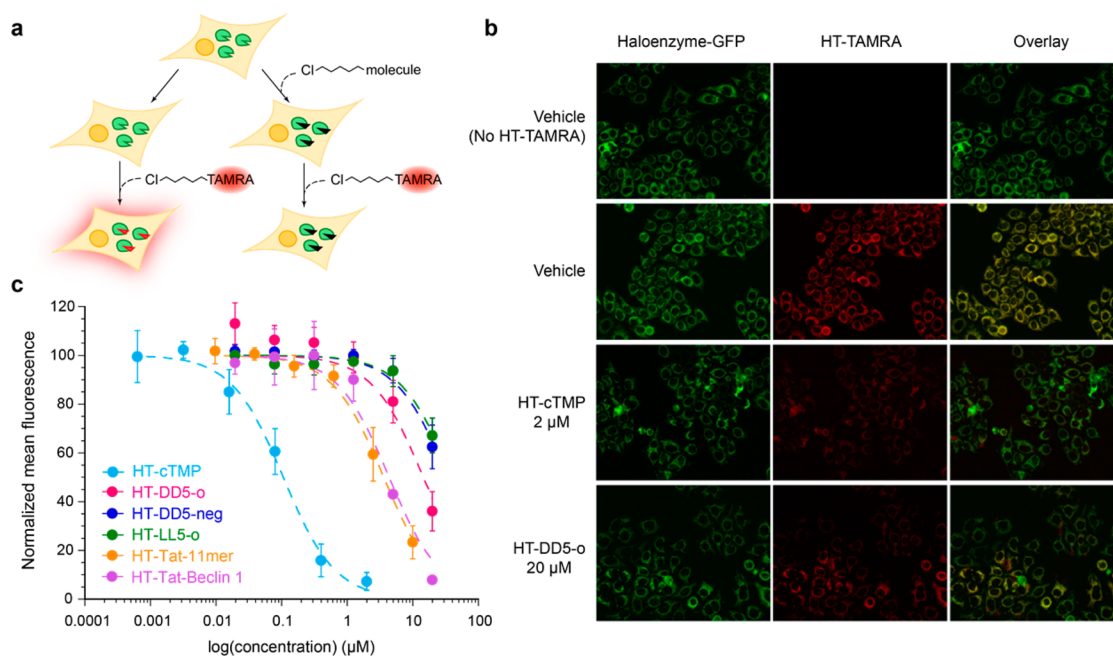
Figure 5. Chloroalkane penetration assay (CAPA) quantitates relative cytosolic access of exogenously added molecules. (a) Schematic showing the experimental procedure of CAPA, which uses a haloenzyme-GFP-expressing HeLa cell line.[63] Untreated cells labeled with HT-TAMRA showed a large increase in red fluorescence as measured by flow cytometry. For CAPA, cells are pretreated with HT-conjugated peptide and then washed and chased with HT-TAMRA. Cell-penetrant molecules react with haloenzyme, blocking its active site and preventing the HT-TAMRA from covalently labeling the cells. (b) Representative images of cells after CAPA, showing haloenzyme-GFP (green) fluorescence, HT-TAMRA (red) fluorescence, and the overlay of the two. The top row shows fluorescence micrographs of cells treated with vehicle (0.2% DMSO) but not HT-TAMRA. The second row shows cells treated with vehicle and HT-TAMRA, which represents 100% of the red signal. The third row shows a representative image of cells treated with HT-cTMP at 2 μM, which have roughly 10% of the red signal. The bottom row shows cells treated with HT-DD5-o at 20 μM, which have roughly 40% of the red signal. (c) Dose-dependence of HT-TAMRA signal after preincubation with different concentrations of HT-cTMP, HT-DD5-o, HT-DD5-neg (a negatively charged, linear analogue of DD5-o), HT-LL5-o, HT-Tat-11mer, and HT-Tat-Beclin 1. Representative flow cytometry data are provided in SI Figure 17. Mean fluorescence from counting 10 000 cells for each sample at each concentration were normalized using the values obtained for vehicle (100% signal) and for vehicle with no HT-TAMRA added (0% signal). Points are means from three independent CAPA experiments, and error bars show standard deviation.

12), allowing complete assignment. Chemical shifts deviated from random coil values in a manner consistent with an overall helical structure (SI Table 2 and SI Figure 13a). NOEs between ($i,i+1$) amide protons were also observed from D-Cys2 to Trp9, consistent with an uninterrupted helical structure across nearly the entire length of the peptide. Medium-range and long-range NOEs also spanned the entire length of the peptide (Figure 4a). These data indicated a high degree of structure both in the N-terminal, stapled portion and in the C-terminal portion. An ensemble of the 25 lowest-energy structures from simulated annealing simulations (Figure 4b) showed tight agreement, with a well-structured, helical backbone (backbone RMSD = 0.44 Å, all-heavy-atom RMSD = 1.1 Å). Circular dichroism experiments revealed a helical signature (SI Figure 13b), confirming that DD5-o forms a robust α-helix in methanol. Methanol can be helix-inducing, so the structure of DD5-o in water could be different, or less well-ordered. We used molecular dynamics simulations of DD5-o in explicit water to provide initial evidence that the NMR-derived structure might be at least a local minimum in aqueous solution. DD5-o retained helical structure after 100 ns of simulation, and the results (shown in SI movie 1 and SI Figures 14 and 15) revealed dynamics of this new class of stapled helix.

A New Assay for Measuring Relative Cytosolic Access. Our data support a mode of action in which autophagy-inducing peptides act at the stage of autophagy initiation.[23,55] Because autophagosome formation is associated with the

cytosolic surfaces of the endoplasmic reticulum and other organelles, it was critical to verify that DD5-o reaches the cytosol.[39,57−59] To this end, we developed a novel cell penetration assay to quantify the cytosolic delivery of DD5-o. The assay, called the ChloroAlkane Penetration Assay (CAPA), is inexpensive, quantitative, and high-throughput and measures cytosolic access without interference from endosomally trapped peptide (Figure 5).

CAPA uses a HeLa cell line that stably expresses a haloenzyme-GFP fusion that is cytosolically oriented. Haloenzyme is a modified bacterial chloroalkane dehydrogenase that covalently labels itself with an otherwise inert chloroalkane functional group; collectively these are known as the HaloTag system.[60−62] In CAPA, the cells are incubated with a molecule of interest that has been conjugated to the chloroalkane (denoted HT-molecule), cells are washed to remove excess HT-molecule, and then extent of penetration is quantitated by reading out the amount of free haloenzyme. If the HT-molecule reaches the cytosol, it reacts with the haloenzyme and blocks its active site, resulting in lower levels of free haloenzyme. The amount of unreacted haloenzyme was measured by exposing cells to the chloroalkane-conjugated dye HT-TAMRA and quantifying red fluorescence using flow cytometry. The red signal reports directly on the amount of free haloenzyme, which is inversely proportional to the degree to which the HT-molecule accessed the cytosol during the incubation period.
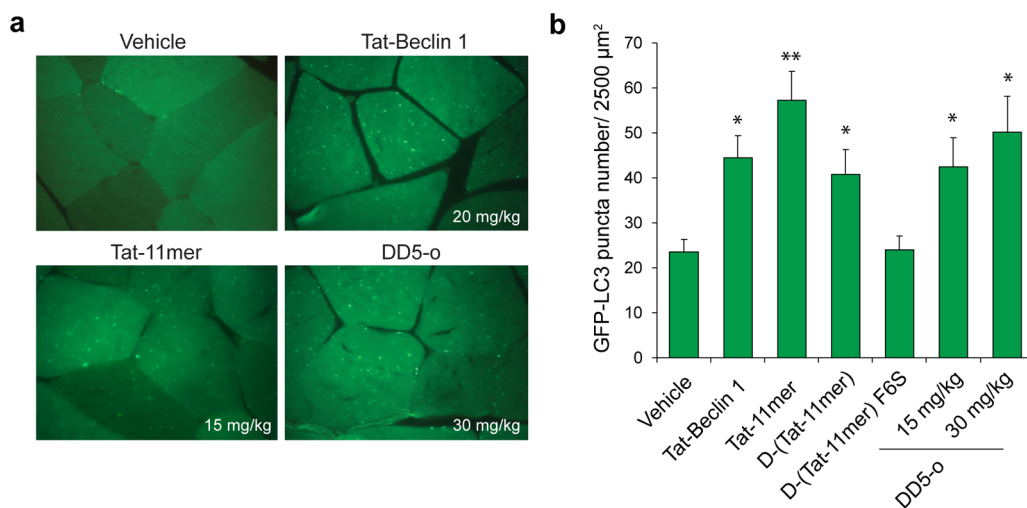
Figure 6. Autophagy induction observed in vivo. (a) Representative images of muscle tissue sections from GFP-LC3 mice treated with vehicle or peptide at 20 mg/kg for Tat-Beclin 1, 15 mg/kg for Tat-11mer and its analogues, and 15 mg/kg and 30 mg/kg for DD5-o. Tissue was analyzed 6 h after intraperitoneal injection of peptide. (b) GFP-LC3 puncta counted per 2500 μm^2 of muscle tissue. A minimum of ten fields was counted per tissue section. Bars represent mean ± SEM for four mice. * denotes $P < 0.05$ and ** denotes $P < 0.01$ by t test for indicated group vs DMSO control.

We first evaluated CAPA with HT-cTMP, a small molecule previously used as a tool for cytosolic protein localization.[63] By flow cytometry and fluorescence microscopy, we observed that preincubation with HT-cTMP suppressed up to 90% of the HT-TAMRA signal. Fluorescence microscopy confirmed that the HT-TAMRA colocalized with the cytosolically oriented GFP-haloenzyme (Figure 5b), and the extent of inhibition was dose-dependent with respect to amount of the HT-cTMP used in the incubation step (Figure 5c). These experiments confirmed that the relative decrease in red fluorescence signal correlated with the amount of HT-molecule that accessed the cytosol during the incubation step.

Next, we synthesized HT-DD5-o, in which the DD5-o sequence was N-terminally capped with the chloroalkane group. p62 and LC3 immunoblot assays verified that HT-DD5-o induced autophagy similarly to the original DD5-o (SI Figure 16). The CAPA data for HT-DD5-o showed dose-dependent suppression of the HT-TAMRA signal (Figure 5c and SI Figure 17). Its dose-dependence curve was similar in shape to HT-cTMP but was shifted 100-fold higher in concentration, as expected for a peptide relative to a small molecule. We also tested a negatively charged, linear variant, HT-DD5-neg, which exhibited cytosolic entry only at high concentration and at the limit of solubility (Figure 5c). The stereoisomer LL5-o was also tested in this assay. HT-LL5-o was found to enter only at high concentrations, similar to the linear, negatively charged variant. Finally, we tested chloroalkane-conjugated versions of Tat-linked peptides using CAPA. HT-Tat-Beclin 1 and HT-Tat-11mer were found to enter the cytosol 2.5-fold and 4-fold better than HT-DD5-o, respectively. Overall, these results directly confirm the cytosolic localization of these autophagy-inducing peptides.

Tat-11mer and DD5-o Activate Autophagy in Vivo and Clear Huntingtin Aggregates in Vitro. Despite its micromolar potency, the Tat-Beclin 1 peptide has shown efficacy in several animal models of human disease.[25−34] To examine whether Tat-11mer and DD5-o have similar in vivo activity, we tested their ability to induce autophagy in GFP-LC3 transgenic mice as described.[23,64] Peptides were delivered via intraperitoneal injection, and after 6 h, muscle tissue was collected. GFP-LC3 puncta were imaged in thin sections and counted by an observer blinded to experimental condition. Tat-11mer produced the largest increase in autophagosome formation, with Tat-Beclin 1 and DD5-o both producing robust increases in autophagosome formation (Figure 6). DD5-o induced autophagy at 15 and 30 mg/kg in a dose-dependent manner. Previous results showed that a *retro-inverso* version of full-length Tat-Beclin 1 also possessed autophagy-inducing activity in vivo.[23] Here, we tested a *retro-inverso* version of Tat-11mer, and this D-amino acid peptide induced autophagy to an extent similar to that for original Tat-Beclin 1 (Figure 6b). A control *retro-inverso* sequence with a Phe6 to Ser substitution had no effect on autophagy. Overall, the in vivo autophagy induction results matched the trends observed for in vitro data.

Along with proteasomal degradation, autophagy is the major pathway by which aggregated proteins are removed from the cytosol. Increasing autophagy leads to the reduction of aggregated protein, reversing a characteristic feature of polyglutamine disorders such as Huntington's disease.[65] We thus tested whether our peptides would help clear protein aggregates from HeLa cells expressing a polyglutamine-expanded huntingtin exon 1 (htt103Q fused to CFP for imaging) from a doxycycline-repressible promoter.[23,65] In this model of protein aggregation, autophagy has been shown to clear small aggregates, but not large (>1 μm) aggregates.[66] Treatment with 20 μM Tat-Beclin 1 was previously shown to decrease the number of small, but not large, htt103Q aggregates, consistent with autophagy-mediated protein turnover.[23] We found that treatment with 20 μM DD5-o or 10 μM Tat-11mer led to a significant decrease in the percentage of cells that have small aggregates and in the number of small aggregates observed per cell (SI Figure 18). Both peptides had potency similar to or greater than that of the full-length Tat-Beclin 1. Control peptides, including LL5-o and a sequence-scrambled version of Tat-11mer, produced no significant clearance of aggregates.

■ DISCUSSION

First reported in 2013, the autophagy-inducing peptide Tat-Beclin 1 has become a critical tool for exploring the therapeutic

potential of autophagy activation.[23,25−32] Here, we describe two new autophagy-inducing peptides based on Tat-Beclin 1. The first, Tat-11mer, has greater potency than the original peptide, and the second, DD5-o, is slightly less potent but does not require a polycationic sequence for cell penetration. Structure−activity relationships revealed conserved residues among these Beclin 1-derived sequences, suggesting that they operate via the same mechanism, which is yet unknown. Notably, the conserved residue Trp2 in Tat-11mer is replaced by a cross-linked D-Cys in DD5-o, suggesting that the hydrophobic staple may functionally replace this part of the conserved sequence. Going forward, its smaller size and intrinsic cell penetration make DD5-o a promising starting point for the development of peptide and small-molecule therapeutics.

DD5-o was developed using a diversity-oriented stapling strategy that scans different structures by varying several aspects of staple position, length, and stereochemistry. Similar chemistry has been applied to phage display libraries and to the design of protein−protein interaction inhibitors and can incorporate further diversity using alternative linkers or artificial thiol-containing amino acids.[51,52,67,68] Here we used this approach to convert an 10-mer peptide with minimal activity into a cell-penetrant stapled peptide with potent autophagy-inducing activity in vitro and in vivo. Previous work had shown that bis-alkylation of L-cysteines at $(i,i+4)$ positions using the m-xylene linker can stabilize α-helical structure.[69] This matches the staple geometry and spacing in DD6-m (Figure 2b), supporting the possibility that DD6-m is also helical, though the staple connects two D-cysteines instead of two L-cysteines. The staple within DD5-o is an $(i,i+3)$ staple that links two D-cysteines with an o-xylene group (Figure 2b). This is an unusual staple geometry that was not suggested by prior helix-stapling chemistries and configurations. Specifically, while $(i,i+3)$ staples of various chemistries have been reported, these reports do not examine the compatibility of helical structure with stapling of two D-amino acids at $(i,i+3)$ positions.[48,70−73] Another relevant feature of DD5-o is an extended hydrophobic surface of over 750 Å^2 which includes the staple and the required hot spot residues. This hydrophobic surface wraps around more than half of the helix (Figure 4c). Having an extended hydrophobic surface was recently found to be critical for cell penetration of hydrocarbon-stapled helices. In fact, DD5-o matches all the biophysical criteria recently described for cell-penetrant stapled helices.[37,74]

To directly measure cell penetration of DD5-o, we developed a novel assay that measures cytosolic localization using the HaloTag system. The most common method currently used to judge cell penetration is to monitor the uptake of dye-labeled molecules by microscopy or flow cytometry.[37,74] This method has difficulty distinguishing material that is trapped in endosomes from material in the cytosol, and it is prone to additional artifacts including peptide aggregation, leakage of peptide after fixation,[75,76] and light-induced redistribution from endosomes to the cytosol.[77] Several groups have developed alternative assays, including dye-mediated assays that produce signals based on changing chemical environment,[78,79] transcriptional readouts using dexamethasone-tagged peptides,[80] and fluorescence correlation spectroscopy for localizing signals in femtoliter volumes within the cell.[81] CAPA improves on these assays in several ways. First, it requires a smaller chemical tag. We found that attachment of various organic dyes to DD5-o led to poor solubility, whereas HT-DD5-o was equally soluble as DD5-o. Second, because the HeLa cells stably express

haloenzyme fused to a cytosolically oriented protein domain, any signal dependent on the haloenzyme reports exclusively on cytosolic access of the HT-molecule. Third, the assay is highly quantitative. Control experiments revealed that up to 90% of the overall signal could be suppressed by preincubation with a cell-penetrant, chloroalkane-conjugated small molecule. The remaining 10% may be due to haloenzyme expressed during the subsequent dye incubation and wash steps. Finally, the readout is high-throughput and does not require specialized microscopy or image analysis techniques. We acquired CAPA data in 96-well plates using a benchtop flow cytometer, and further miniaturization and alternate readouts are possible.

CAPA allowed direct quantitation of the dose-dependence of cell penetration for autophagy-inducing peptides. Importantly, these dose dependences closely matched the dose-dependences of autophagy induction. These data imply that potency is currently limited by cell penetration, and that improving cell penetration will improve overall activity. The ability to quantitate cell penetration in a high-throughput manner will greatly accelerate development of these and other potential peptide therapeutics. In fact, CAPA can be directly applied to any chemically tractable molecule, including small molecules, peptides, proteins, nucleic acids, antibodies, viral particles, and nanoparticles. Because the haloenzyme is genetically introduced, it can be directed to any cellular compartment, enabling separate CAPA measurements of access to different cellular compartments and organelles.

Finally, the cumulative structure-activity relationships of all the Beclin 1-derived peptides, the structure of DD5-o in methanol, and the activity of *retro-inverso* variants of Tat-Beclin 1 and Tat-11mer provide multiple independent lines of evidence that Beclin 1-derived peptides might be active in helical conformations. This finding is in stark contrast with the published structure of the Beclin 1 ECD and current models of Beclin 1 complexes.[44,55,56] If helical structure is important for Beclin 1-derived peptides, this would raise new questions about the structure and function of the BARA domains of Beclin 1. Further studies on Beclin 1 will be necessary to determine whether this domain assumes a helical structure in the autophagosome initiation complex, or whether it converts to a helical structure when binding other autophagy regulators. We expect these and other Beclin 1-derived peptides will continue to reveal molecular details of autophagy induction and regulation, and will continue to serve as potent tools and potential lead compounds for examining the effects of autophagy induction on human disease.

■ EXPERIMENTAL METHODS

Reagents and Antibodies. Fmoc-amino acids were purchased from ChemPep or Anaspec. Rink Amide resin was purchased from ChemPep. Dibromo-linkers and *N,N*-dimethylformamide were purchased from Sigma-Aldrich. Acetonitrile was purchased from Fisher Scientific. Materials for cell culture were purchased from Thermo Scientific. For immunoblot experiments rabbit anti-LC3 (1:1000 dilution, Novus Biologicals), guinea-pig anti-p62 (1:800 dilution, Progen), mouse monoclonal anti-actin (1:2000 dilution, Santa Cruz), and goat anti-rabbit IgG (1:2000 dilution, Santa Cruz) were used.

Peptide Synthesis and Thioether Stapling. Peptides were synthesized on Rink Amide resin (0.53 mmol/g) using standard Fmoc chemistry. For each coupling 5 equiv of Fmoc-amino acid or carboxylic acid, 5 equiv of 2-(7-aza-1*H*-benzo- triazole-1-yl)-1,1,3,3-tetramethyluronium hexafluorophosphate (HATU), 5 equiv of 1-hydroxy-7-azabenzotriazole (HOAt), and 13 equiv of diisopropylethylamine

(DIPEA) were dissolved in *N,N*-dimethylformamide (DMF) and added to the resin. The reaction was allowed to proceed for 30 min. For the N-terminal caps, double coupling was required. For chloroalkane-conjugated peptides, chloroalkane carboxylic acid (kindly provided by the Chenoweth Lab at University of Pennsylvania) was coupled to the N-terminus by reacting 3 equiv with 3 equiv benzotriazol-1-yl-oxytripyrrolidino phosphonium hexafluorophosphate (PyBOP), 3 equiv 1-hydroxybenzotriazole (HOBt), and 6 equiv DIPEA for 1 h at room temperature. The peptides were globally deprotected and cleaved off the resin by treatment with 94:2.5:2.5:1 (v/v) TFA/ethanedithiol/water/triisipropylsilane for 3 h. The peptides were triturated in cold diethyl ether and washed twice with cold ether. The crude pellet was dried and then dissolved in 50:50 acetonitrile/water. After the identity of the major product was confirmed by MALDI-TOF mass spectrometry, peptides were subjected to bis-alkylation conditions as described.[52] All peptides were purified by reverse-phase HPLC on a C_8 preparative column. Purity of the final product was confirmed on a C_{18} analytical column and observed masses of final products are given in SI Table 1.

Immunoblot Assays. Cells were treated with peptide in Opti-MEM (Thermo Scientific) acidified with 0.15% (v/v) 6 N HCl for 2 h. Cells were rinsed with phosphate-buffered saline (PBS) and lysed in lysis buffer (20 mM HEPES, 150 mM NaCl, 1 mM EDTA, 1% Triton X-100, Roche protease inhibitor cocktail) on ice for 1 h. Cell lysates were centrifuged at 16 000 g for 10 min at 4 °C, and supernatants were separated by SDS-PAGE and transferred to PVDF membranes. The membranes were blocked in 5% nonfat dry milk (NFDM) in PBST (PBS + 0.05% Tween-20) for 1 h and then incubated overnight at 4 °C with primary antibody in 5% NFDM in PBST. The blots were washed with PBST and incubated with HRP-conjugated secondary antibodies diluted in 5% NFDM in PBST for 1 h at room temperature. Membranes were washed with PBST and visualized with SuperSignal West Pico Chemiluminescent Substrate (Thermo Scientific).

GFP-LC3 in Vitro and in Vivo Experiments. HeLa/GFP-LC3 cells were generated as previously shown,[23] and treated with peptides for 2 h as described above. Cells were fixed with 2% paraformaldehyde (PFA) in PBS, and GFP-LC3 puncta per cell were counted and quantified as described.[82] To measure autophagy in mouse tissues, 6-week-old GFP-LC3 transgenic mice[64] (two males and two females per experimental group) were injected intraperitoneally with Tat-Beclin 1 (20 mg/kg), Tat-11mer (15 mg/kg), D-(Tat-11mer) (15 mg/kg), D-(Tat-11mer-F6S) (15 mg/kg), or DD5-o (15 or 30 mg/kg). After 6 h, mice were sacrificed and fixed by perfusion with 4% PFA in PBS. Tissues were fixed in 4% PFA overnight, 15% sucrose for 4 h, and 30% sucrose overnight before frozen sections were prepared and used for fluorescence microscopy analysis as described.[9] GFP-LC3 puncta were quantified per 2500 μm^2 of tissue using fluorescence microscopy by an observer blinded to experimental condition. Animal experiments were approved by the UTSW Institutional Animal Care Use Committee and performed in accordance with institutional guidelines.

Htt Aggregate Assay. HeLa-Htt103Q cells were cultured as described previously.[65] For the Htt103Q aggregate assay, cells were fixed with 2% PFA in PBS and CFP-positive aggregates <1 μm were counted using fluorescence microscopy by an observer blinded to experimental condition.

Chloroalkane Penetration Assay. HaLo-GFP-Mito HeLa cells were provided by the Chenoweth Lab.[63] Cells were cultured using DMEM + 10% FBS + 1% Pen/Strep +1 $\mu g/mL$ puromycin. For experiments, cells were seeded in a 24- or 48-well plate the day before at 1.0×10^5 cells/well. Cells were rinsed with PBS and then treated with peptides in acidified Opti-MEM (0.15% 6 N HCl) for 4 h. Media was aspirated and cells were washed for 30 min with phenol red-free Opti-MEM. Cells were then incubated with 5 μM HT-TAMRA (HTag-TMR, Promega) in phenol red-free Opti-MEM for 30 min. Cells were washed for 15 min with phenol red-free DMEM + 10% FBS + 1% pen/strep. Cells were rinsed with PBS and then trypsinized and transferred to microcentrifuge tubes. Cells were pelleted and washed twice with PBS. Cell pellets were resuspended in 250 μL of PBS, and 200 μL was transferred to 96-well plates for flow cytometry analysis using a Guava EasyCyte 6HT-2L benchtop flow cytometer. Data was

gated for live cells and 10 000 cells were measured per sample. Mean fluorescence intensity was calculated from raw data, and these values were normalized using samples with no dye added (0% red signal) and samples with dye added but no HT-molecule added in the preincubation step (100% red signal).

ASSOCIATED CONTENT

Ⓢ Supporting Information

The Supporting Information is available free of charge on the ACS Publications website at DOI: 10.1021/jacs.7b01698.

Molecular dynamics simulations for DD5-o in water (AVI)

Peptide chemical structures and sequences, supplementary Western Blots, Htt103Q aggregation assay data, and NMR data for peptide DD5-o (PDF)

AUTHOR INFORMATION

Corresponding Authors
*beth.levine@utsouthwestern.edu
*joshua.kritzer@tufts.edu

ORCID Ⓞ
Kamlesh M. Makwana: 0000-0002-4918-8572
Joshua A. Kritzer: 0000-0003-2878-6781

Notes
The authors declare no competing financial interest.

REFERENCES

(1) Yoshimori, T. *Biochem. Biophys. Res. Commun.* **2004**, *313*, 453.
(2) Reggiori, F.; Komatsu, M.; Finley, K.; Simonsen, A. *Int. J. Cell Biol.* **2012**, *2012*, 1.
(3) Levine, B.; Klionsky, D. J. *Dev. Cell* **2004**, *6*, 463.
(4) Yorimitsu, T.; Klionsky, D. J. *Cell Death Differ.* **2005**, *12*, 1542.
(5) Menzies, F. M.; Fleming, A.; Rubinsztein, D. C. *Nat. Rev. Neurosci.* **2015**, *16*, 345.
(6) Liang, X. H.; Jackson, S.; Seaman, M.; Brown, K.; Kempkes, B.; Hibshoosh, H.; Levine, B. *Nature* **1999**, *402*, 672.
(7) Yue, Z.; Jin, S.; Yang, C.; Levine, A. J.; Heintz, N. *Proc. Natl. Acad. Sci. U. S. A.* **2003**, *100*, 15077.
(8) Tang, H.; Sebti, S.; Titone, R.; Zhou, Y.; Isidoro, C.; Ross, T. S.; Hibshoosh, H.; Xiao, G.; Packer, M.; Xie, Y.; Levine, B. *EBioMedicine* **2015**, *2*, 255.
(9) Qu, X.; Yu, J.; Bhagat, G.; Furuya, N.; Hibshoosh, H.; Troxel, A.; Rosen, J.; Eskelinen, E. L.; Mizushima, N.; Ohsumi, Y.; Cattoretti, G.; Levine, B. *J. Clin. Invest.* **2003**, *112*, 1809.
(10) Mizushima, N.; Komatsu, M. *Cell* **2011**, *147*, 728.
(11) Kim, K. H.; Lee, M.-S. *Nat. Rev. Endocrinol.* **2014**, *10*, 322.
(12) Levine, B.; Mizushima, N.; Virgin, H. W. *Nature* **2011**, *469*, 323.
(13) Rubinsztein, D. C.; Mariño, G.; Kroemer, G. *Cell* **2011**, *146*, 682.
(14) Mizushima, N.; Levine, B.; Cuervo, A. M.; Klionsky, D. J. *Nature* **2008**, *451*, 1069.
(15) Rubinsztein, D. C.; Codogno, P.; Levine, B. *Nat. Rev. Drug Discovery* **2012**, *11*, 709.
(16) Levine, B.; Liu, R.; Dong, X.; Zhong, Q. *Trends Cell Biol.* **2015**, *25*, 533.

(17) Cheng, Y.; Ren, X.; Hait, W. N.; Yang, J. *Pharmacol. Rev.* **2013**, *65*, 1162.

(18) Muciño, G.; Castro-Obregón, S.; Hernandez-Pando, R.; Del Rio, G. *IUBMB Life* **2016**, *68*, 259.

(19) Levine, B.; Packer, M.; Codogno, P. *J. Clin. Invest.* **2015**, *125*, 14.

(20) Zhong, Z.; Sanchez-Lopez, E.; Karin, M. *Cell* **2016**, *166*, 288.

(21) Kihara, a; Kabeya, Y.; Ohsumi, Y.; Yoshimori, T. *EMBO Rep.* **2001**, *2*, 330.

(22) Kyei, G. B.; Dinkins, C.; Davis, A. S.; Roberts, E.; Singh, S. B.; Dong, C.; Wu, L.; Kominami, E.; Ueno, T.; Yamamoto, A.; Federico, M.; Panganiban, A.; Vergne, I.; Deretic, V. *J. Cell Biol.* **2009**, *186*, 255.

(23) Shoji-Kawata, S.; Sumpter, R., Jr; Leveno, M.; Campbell, G. R.; Zou, Z.; Kinch, L.; Wilkins, A. D.; Sun, Q.; Pallauf, K.; MacDuff, D.; Huerta, C.; Virgin, H. W.; Helms, J. B.; Eerland, R.; Tooze, S. A.; Xavier, R.; Lenschow, D. J.; Yamamoto, A.; King, D.; Lichtarge, O.; Grishin, N. V.; Spector, S. A.; Kaloyanova, D. V.; Levine, B. *Nature* **2013**, *494*, 201.

(24) Liang, X. H.; Kleeman, L. K.; Jiang, H. H.; Gordon, G.; Goldman, J. E.; Berry, G.; Herman, B.; Levine, B.; Hill, C.; Carolina, N. *J. Virol.* **1998**, *72*, 8586.

(25) Miao, Y.; Li, G.; Zhang, X.; Xu, H.; Abraham, S. N. *Cell* **2015**, *161*, 1306.

(26) Kobayashi, S.; Orba, Y.; Yamaguchi, H.; Takahashi, K.; Sasaki, M.; Hasebe, R.; Kimura, T.; Sawa, H. *Virus Res.* **2014**, *191*, 83.

(27) Hakata, Y.; Tsuchiya, S.; Michiue, H.; Ohtsuki, T.; Matsui, H.; Miyazawa, M.; Kitamatsu, M. *Chem. Commun.* **2015**, *51*, 413.

(28) Pietrocola, F.; Pol, J.; Vacchelli, E.; Rao, S.; Enot, D. P.; Baracco, E. E.; Levesque, S.; Castoldi, F.; Jacquelot, N.; Yamazaki, T.; Senovilla, L.; Marino, G.; Aranda, F.; Durand, S.; Sica, V.; Chery, A.; Lachkar, S.; Sigl, V.; Bloy, N.; Buque, A.; Falzoni, S.; Ryffel, B.; Apetoh, L.; Di Virgilio, F.; Madeo, F.; Maiuri, M. C.; Zitvogel, L.; Levine, B.; Penninger, J. M.; Kroemer, G. *Cancer Cell* **2016**, *30*, 147.

(29) Livingston, M. J.; Ding, H.-F.; Huang, S.; Hill, J. A.; Yin, X.-M.; Dong, Z. *Autophagy* **2016**, *12*, 976.

(30) Liu, Y.; Shoji-Kawata, S.; Sumpter, R. M.; Wei, Y.; Ginet, V.; Zhang, L.; Posner, B.; Tran, K. A.; Green, D. R.; Xavier, R. J.; Shaw, S. Y.; Clarke, P. G. H.; Puyal, J.; Levine, B. *Proc. Natl. Acad. Sci. U. S. A.* **2013**, *110*, 20364.

(31) Wang, S.; Livingston, M. J.; Su, Y.; Dong, Z. *Autophagy* **2015**, *11*, 607.

(32) Sosulski, M. L.; Gongora, R.; Danchuk, S.; Dong, C.; Luo, F.; Sanchez, C. G. *Aging Cell* **2015**, *14*, 774.

(33) Shirakabe, A.; Zhai, P.; Ikeda, Y.; Saito, T.; Maejima, Y.; Hsu, C. P.; Nomura, M.; Egashira, K.; Levine, B.; Sadoshima, J. *Circulation* **2016**, *133*, 1249.

(34) Zhu, P.; Sieben, C. J.; Xu, X.; Harris, P. C.; Lin, X. *Hum. Mol. Genet.* **2017**, *26*, 158.

(35) Cardozo, A. K.; Buchillier, V.; Mathieu, M.; Chen, J.; Ortis, F.; Ladriere, L.; Allaman-Pillet, N.; Poirot, O.; Kellenberger, S.; Beckmann, J. S.; Eizirik, D. L.; Bonny, C.; Maurer, F. *Biochim. Biophys. Acta, Biomembr.* **2007**, *1768*, 2222.

(36) Quartararo, J. S.; Eshelman, M. R.; Peraro, L.; Yu, H.; Baleja, J. D.; Lin, Y.-S.; Kritzer, J. a. *Bioorg. Med. Chem.* **2014**, *22*, 6387.

(37) Chu, Q.; Moellering, R. E.; Hilinski, G. J.; Kim, Y.; Grossmann, T. N.; Yeh, J. T.-H.; Verdine, G. L. *MedChemComm* **2015**, *6*, 111.

(38) Walensky, L. D.; Bird, G. H. *J. Med. Chem.* **2014**, *57*, 6275.

(39) Milletti, F. *Drug Discovery Today* **2012**, *17*, 850.

(40) Lau, Y. H.; de Andrade, P.; Wu, Y.; Spring, D. R. *Chem. Soc. Rev.* **2015**, *44*, 91.

(41) Gavenonis, J.; Jonas, N. E.; Kritzer, J. A. *Bioorg. Med. Chem.* **2014**, *22*, 3989.

(42) Hill, T. A.; Shepherd, N. E.; Diness, F.; Fairlie, D. P. *Angew. Chem., Int. Ed.* **2014**, *53*, 13020.

(43) Zou, Y.; Spokoyny, A. M.; Zhang, C.; Simon, M. D.; Yu, H.; Lin, Y.-S.; Pentelute, B. L. *Org. Biomol. Chem.* **2014**, *12*, 566.

(44) Huang, W.; Choi, W.; Hu, W.; Mi, N.; Guo, Q.; Ma, M.; Liu, M.; Tian, Y.; Lu, P.; Wang, F.-L.; Deng, H.; Liu, L.; Gao, N.; Yu, L.; Shi, Y. *Cell Res.* **2012**, *22*, 473.

(45) Mizushima, N.; Yoshimori, T.; Levine, B. *Cell* **2010**, *140*, 313.

(46) Klionsky, D. J.; Abdelmohsen, K.; Abe, A.; Abedin, M. J.; Abeliovich, H.; Acevedo Arozena, A.; Adachi, H.; Adams, C. M.; Adams, P. D.; Adeli, K.; et al. *Autophagy* **2016**, *12*, 1.

(47) Timmerman, P.; Beld, J.; Puijk, W. C.; Meloen, R. H. *ChemBioChem* **2005**, *6*, 821.

(48) Jo, H.; Meinhardt, N.; Wu, Y.; Kulkarni, S.; Hu, X.; Low, K. E.; Davies, P. L.; Degrado, W. F.; Greenbaum, D. C. *J. Am. Chem. Soc.* **2012**, *134*, 17704.

(49) Timmerman, P.; Puijk, W. C.; Meloen, R. H. *J. Mol. Recognit.* **2007**, *20*, 283–299.

(50) Smeenk, L. E. J.; Dailly, N.; Hiemstra, H.; van Maarseveen, J. H.; Timmerman, P. *Org. Lett.* **2012**, *14*, 1194.

(51) Siegert, T. R.; Bird, M. J.; Makwana, K. M.; Kritzer, J. A. *J. Am. Chem. Soc.* **2016**, *138*, 12876.

(52) Peraro, L.; Siegert, T. R.; Kritzer, J. A. *Methods Enzymol.* **2016**, *580*, 303.

(53) Yamamoto, A.; Tagawa, Y.; Yoshimori, T.; Moriyama, Y.; Masaki, R.; Tashiro, Y. *Cell Struct. Funct.* **1998**, *23*, 33.

(54) He, C.; Klionsky, D. J. *Annu. Rev. Genet.* **2009**, *43*, 67.

(55) Baskaran, S.; Carlson, L.-A.; Stjepanovic, G.; Young, L. N.; Kim, D. J.; Grob, P.; Stanley, R. E.; Nogales, E.; Hurley, J. H. *eLife* **2014**, *3*, 05115.

(56) Rostislavleva, K.; Soler, N.; Ohashi, Y.; Zhang, L.; Pardon, E.; Burke, J. E.; Masson, G. R.; Johnson, C.; Steyaert, J.; Ktistakis, N. T.; Williams, R. L. *Science* **2015**, *350*, aac7365.

(57) Madani, F.; Lindberg, S.; Langel, U.; Futaki, S.; Gräslund, A. *J. Biophys.* **2011**, *2011*, 414729.

(58) Erazo-Oliveras, A.; Muthukrishnan, N.; Baker, R.; Wang, T. Y.; Pellois, J. P. *Pharmaceuticals* **2012**, *5*, 1177.

(59) Bechara, C.; Sagan, S. *FEBS Lett.* **2013**, *587*, 1693.

(60) Lang, C.; Schulze, J.; Mendel, R. R.; Hänsch, R. *J. Exp. Bot.* **2006**, *57*, 2985.

(61) Los, G. V.; Encell, L. P.; McDougall, M. G.; Hartzell, D. D.; Karassina, N.; Zimprich, C.; Wood, M. G.; Learish, R.; Ohana, R. F.; Urh, M.; Simpson, D.; Mendez, J.; Zimmerman, K.; Otto, P.; Vidugiris, G.; Zhu, J.; Darzins, A.; Klaubert, D. H.; Bulleit, R. F.; Wood, K. V. *ACS Chem. Biol.* **2008**, *3*, 373.

(62) Friedman Ohana, R.; Kirkland, T. A.; Woodroofe, C. C.; Levin, S.; Uyeda, H. T.; Otto, P.; Hurst, R.; Robers, M. B.; Zimmerman, K.; Encell, L. P.; Wood, K. V. *ACS Chem. Biol.* **2015**, *10*, 2316.

(63) Ballister, E. R.; Aonbangkhen, C.; Mayo, A. M.; Lampson, M. A.; Chenoweth, D. M. *Nat. Commun.* **2014**, *5*, 5475.

(64) Mizushima, N.; Yamamoto, A.; Matsui, M.; Yoshimori, T.; Ohsumi, Y. *Mol. Biol. Cell* **2004**, *15*, 1101.

(65) Yamamoto, A.; Cremona, M. L.; Rothman, J. E. *J. Cell Biol.* **2006**, *172*, 719.

(66) Harris, H.; Rubinsztein, D. C. *Nat. Rev. Neurol.* **2011**, *8*, 108.

(67) Chen, S.; Gopalakrishnan, R.; Schaer, T.; Marger, F.; Hovius, R.; Bertrand, D.; Pojer, F.; Heinis, C. *Nat. Chem.* **2014**, *6*, 1009.

(68) Wang, Y.; Chou, D. H.-C. *Angew. Chem., Int. Ed.* **2015**, *54*, 10931.

(69) Jo, H.; Meinhardt, N.; Wu, Y.; Kulkarni, S.; Hu, X.; Low, K. E.; Davies, P. L.; DeGrado, W. F.; Greenbaum, D. C. *J. Am. Chem. Soc.* **2012**, *134*, 17704.

(70) Muppidi, A.; Zhang, H.; Curreli, F.; Li, N.; Debnath, A. K.; Lin, Q. *Bioorg. Med. Chem. Lett.* **2014**, *24*, 1748.

(71) Walensky, L. D.; Kung, A. L.; Escher, I.; Malia, T. J.; Barbuto, S.; Wright, R. D.; Wagner, G.; Verdine, G. L.; Korsmeyer, S. J. *Science* **2004**, *305*, 1466.

(72) Bird, G. H.; Irimia, A.; Ofek, G.; Kwong, P. D.; Wilson, I. a; Walensky, L. D. *Nat. Struct. Mol. Biol.* **2014**, *21*, 1058.

(73) Micewicz, E. D.; Sharma, S.; Waring, A. J.; Luong, H. T.; McBride, W. H.; Ruchala, P. *Int. J. Pept. Res. Ther.* **2016**, *22*, 67.

(74) Bird, G. H.; Mazzola, E.; Opoku-Nsiah, K.; Lammert, M. A.; Godes, M.; Neuberg, D. S.; Walensky, L. D. *Nat. Chem. Biol.* **2016**, *12*, 845.

(75) Richard, J. P.; Melikov, K.; Vives, E.; Ramos, C.; Verbeure, B.; Gait, M. J.; Chernomordik, L. V.; Lebleu, B. *J. Biol. Chem.* **2003**, *278*, 585.

(76) Belitsky, J. M.; Leslie, S. J.; Arora, P. S.; Beerman, T. A.; Dervan, P. B. *Bioorg. Med. Chem.* **2002**, *10*, 3313.

(77) Maiolo, J. R.; Ottinger, E. A.; Ferrer, M. *J. Am. Chem. Soc.* **2004**, *126*, 15376.

(78) Mäger, I.; Eiriksodottir, E.; Langel, K.; EL Andaloussi, S.; Langel, U. *Biochim. Biophys. Acta, Biomembr.* **2010**, *1798*, 338.

(79) Qian, Z.; Dougherty, P. G.; Pei, D. *Chem. Commun.* **2015**, *51*, 2162.

(80) Yu, P.; Liu, B.; Kodadek, T. *Nat. Biotechnol.* **2005**, *23*, 746.

(81) Larochelle, J. R.; Cobb, G. B.; Steinauer, A.; Rhoades, E.; Schepartz, A. *J. Am. Chem. Soc.* **2015**, *137*, 2536.

(82) Pattingre, S.; Tassa, A.; Qu, X.; Garuti, R.; Liang, X. H.; Mizushima, N.; Packer, M.; Schneider, M. D.; Levine, B. *Cell* **2005**, *122*, 927.